Journal of Energy Storage 60 (2023) 106630

Contents lists available at ScienceDirect

Journal of Energy Storage

journal homepage: www.elsevier.com/locate/est

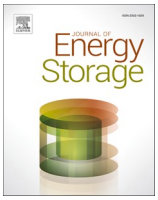

Research Papers

Thermal performance of a hybrid steel-concrete tank section for thermal energy storage in concentrated solar power plants

T. Lucio-Martin [a], M. Martin [b], L. Guerreiro [c], R.S. Villardón [b], J. Lopez [d], M.C. Alonso [a,*]

[a] Consejo Superior de Investigaciones Científicas, Eduardo Torroja Institute for Construction Sciences (CSIC-IETcc), Serrano Galvache 4, 28033 Madrid, Spain
[b] Ingeniería Especializada Obra Civil e Industrial, S.A, Alcobendas, Spain
[c] Univ. of Evora, ICT, Evora, Portugal
[d] ACCIONA Industrial S.A., Alcobendas, Spain

ARTICLE INFO

Keywords:
Thermocline tank
Concrete
Monitoring
Thermal energy storage
Prototype

ABSTRACT

Several studies of thermocline molten salt tanks have proven to be suitable for thermal energy storage systems. However, there is a lack of experimental investigations performed. The building of a hybrid section and its assessment operating as a thermocline tank are the main objectives of this research work. The novelty is to prove the performance of the hybrid tank concept made of a thick concrete layer and a thin steel liner. The tank section studied comprises the following layers of materials: a steel liner, an air gap interface, a high thermal concrete layer and insulating materials. The thermal response was monitored using thermocouples located between the layers, at different heights and widths of the whole tank section length. The performance during the commissioning (first heat) and the operation (3 heat/cool cycles between 200/500 °C) of the tank section is analysed. The thermal appropriateness of using concrete as part of the thermocline tank has demonstrated the suitability and good thermal response up to 425 °C showing isolating and thermal inertia. The presence of the air gap interface between the steel liner and the concrete generates a heat convection current with local energy gradients along the section height.

1. Introduction

The increase in energy consumption has raised awareness of the research and innovation of new sustainable energy sources [1]. Solar energy plays an important role in the energy transition. However, the intermittence of the solar source has raised the importance of energy storage [2].

Concentrating solar power plants (CSP) commonly store energy in a two-tank system by using molten salts as a storage medium with a useful sensible heat defined by the difference between hot and cold temperature levels [2–5]. Depending on the CSP plant configuration, this storage medium could also be the Heat Transfer Fluid (HTF) of the plant which, once heated, is stored in the hot tank for further use. When the thermal energy stored demands electricity production or process heat, the hot fluid coming from the hot tank is pumped into the system and its energy is transferred through a heat exchanger and returned cold to the cold tank. This two-tank architecture is well established in most CSP plants with storage systems, with direct or indirect schemes, but recent studies have demonstrated the use of a single-one thermocline tank could give better results in terms of overall cost reduction [2,6,7].

In a thermocline tank, the whole storage medium is placed inside the same tank and separated due to natural thermal stratification or using a membrane. In this case, the storage medium is composed of a storage medium (liquid at operating temperatures) and a packed bed system in many cases named filler (solid material). The amount of available thermal energy is directly proportional to the temperature of the packed bed and the storage fluid inside the thermocline tank. In this case, the energy is stored as sensible heat. When the tank is charging energy, the heated molten salts come into the tank from the upper part and displace the thermocline region to the bottom increasing until a limited maximum outlet fluid temperature, named cut-off temperature. At the same time, the cold storage fluid is demanded from the bottom part of the thermocline. In the discharging process, hot molten salt gets out of the tank from the top and the thermocline zone is moved to the top [8], decreasing the packed-bed temperature until the cut-off temperature. Therefore, thermal stratification expansion limits the tank storage capacity.

* Corresponding author at: Consejo Superior de Investigaciones Científicas, Eduardo Torroja Institute for Construction Sciences (CSIC-IETcc), Calle de Serrano Galvache, 4, 28033 Madrid, Spain.
E-mail address: mcalonso@ietcc.csic.es (M.C. Alonso).

https://doi.org/10.1016/j.est.2023.106630
Received 9 September 2022; Received in revised form 2 December 2022; Accepted 4 January 2023
Available online 21 January 2023

Nomenclature

Acronyms

AG	air gap
CAC	Calcium Aluminate Cement
CS	case study
CSP	concentrating solar power
DOD	depth of discharge
HHM	Higher Heating Mat
HTF	Heat Transfer Fluid
I	insulation
IL	interface layer
LHM	Lower Heating Mat
MS	molten salt
SL	steel liner
SLS	Serviceability Limit State
TES	thermal energy storage
ULS	Ultimate Limit State

The main benefit pointed out in the literature about thermocline tank systems is their significant potential value for cost reduction, as considered in [9,10]. Nevertheless, the overall performance efficiency against the two-tank system is lower [11]. Moreover, several authors have studied and techno-economically compared these two different CSP storage systems, revealing construction scaling issues needed to be solved for their final market penetration [12]. It is not just a matter of reducing cost from theoretic, but specific design, construction and operation guidelines and improvements must be achieved for its final commercial deployment.

In particular to the design and construction process to the cost-reduction of the final system, recent studies have analysed the suitability of using concrete as thermal energy storage (TES) material for a TES infrastructure under high-temperature regimes [13–18]. However, the performance has been probed in small concrete specimens and its viability at a bigger scale has not been implemented. There exists a specific brand-new heat storage application where a thermocline was studied for heated particle storage but the concrete is located after the insulation layer and the maximum temperature in the concrete was 93 °C [19]. For this reason the H2020 R&D project Newsol 'New Storage Latent and sensible concept for high efficient CSP plants' aimed at developing materials and TES architectures, such as a thermocline hybrid tank with solid and liquid high thermal storage materials for improving the sustainability of CSP while having a relatively high specific heat [20]. One of the architectures developed has been a thermocline tank constituted of two material layers, one external made of high thermal performance concrete based on CAC (a cement used in special constructions for high-temperature applications) and an internal steel liner as TES infrastructure. Inside the storage thermocline, materials tested were ternary molten salts (CaNaK/NO_3) and waste slag with high iron content as packed bed material for storing thermal energy as filler material inside the thermocline tank.

In this investigation, a prototype section of the designed thermocline tank has been tested to evaluate, assess and optimise its operation. Therefore, the aim has been to evaluate the thermal performance of the thermocline tank section using sensors located between the layers across the prototype tank sections. The innovation of this prototype was the use of a hybrid tank made of a thick layer of high thermal concrete with a thinner steel liner. The section of the thermocline tank studied comprised of different layers, as follows, from the heat source to the external surface in contact with the environment: 1) heating mats simulating the heat coming from the molten salts; 2) a thin steel liner working as a container for the molten salts; 3) interface (Air Gap) to permit the thermal expansions of the molten salt (MS) during the operation; 4) a thick concrete layer as part of the tank infrastructure and 5) insulating materials (rock wool and expanded clay) to minimize the heat losses to the surroundings from walls, tops and bottom foundation of the tank. Fig. 1 includes the details of the overall single-tank designed for heat storage system for which the storage tank-section is being considered.

Given the foregoing, this article aims to improve the knowledge in the construction, as well as in the commissioning and operation of a hybrid section of a thermocline TES infrastructure made of concrete and steel, analysing its technical performance to verify if it could be deployed for large scale storage systems. In short, the prototype testing presented in this article at high temperatures under a thermal cyclic regime provides insights into this type of TES and recommendations for the operation of this hybrid thermocline tank storage technology.

2. Background

2.1. CSP plants with molten salts

The reference case for benchmarking commercial thermal storage systems for CSP plants is the two-tank system. The indirect two-tank storage system is used in several parabolic trough collector plants [2,21], whereas the direct two-tank thermal is used in central receiver plants [2,22] and stores sensible heat using molten salts as a storage medium between 290 and 565 °C. Moreover, recent advances have demonstrated the use of Solar Salt up to 600 °C [2,3,23]. The evolution of the temperature across the layers of the tanks is of interest to assess the heat transfer losses that take place in the infrastructure between the molten salts to the surroundings that finally will define the thermal storage efficiency of the system. Indeed, the infrastructure needs to withstand the heating and cooling cycles at high temperatures, within the temperature range mentioned above.

The temperatures of the "hot" and "cool" molten salts vary depending on several factors such as the type of salt, the CSP technology or the storage type and technology. Regarding the CSP technology, the temperature for storing energy varies for Parabolic Trough Technology, which usually ranges between 280 and 400 °C, in indirect systems using synthetic oil in the primary loop and molten salts as the heat storage medium. Moreover, a pilot facility in Massa Martana, Italy, has demonstrated that molten salt can also be used in a Parabolic Trough Collector as a direct system, achieving temperatures up to 550 °C [24]. On the other hand, in the existing Concentrated Solar Tower Plants, the maximum operating temperature is 565 °C [25], as is the case of Gemasolar as a direct system, a 19 MWe Plant located in Sevilla, Spain [26].

2.2. Molten salts

Concerning R&D on molten salts (MS), recent studies analysed new types of mixes to achieve lower melting points and higher temperature stability to improve the properties of the fluid and, hence, significantly contribute to increasing the thermal energy storage capacity [27]. The common thermal storage medium applied in commercial CSP projects is the so-called "Solar Salt", a mixture with an approximate composition of 60% $NaNO_3$ and 40% KNO_3 [5] that present a high melting point of 223 °C, but some researchers have pointed out the urgent need on reducing this temperature as a path to reduce the cost of this kind of storage systems [2,27,28].

Several studies have demonstrated the viability of using ternary and quaternary mixes to reduce the melting point down to 100–120 °C [29–32]. Nevertheless, the thermal stability of the salts is also reduced up to 480–500 °C [29–32]. On the other hand, a novel ternary molten salt has been patented [33] with a melting point of 131 °C and, therefore, it can be operated in a temperature range between 170 °C and 500 °C.

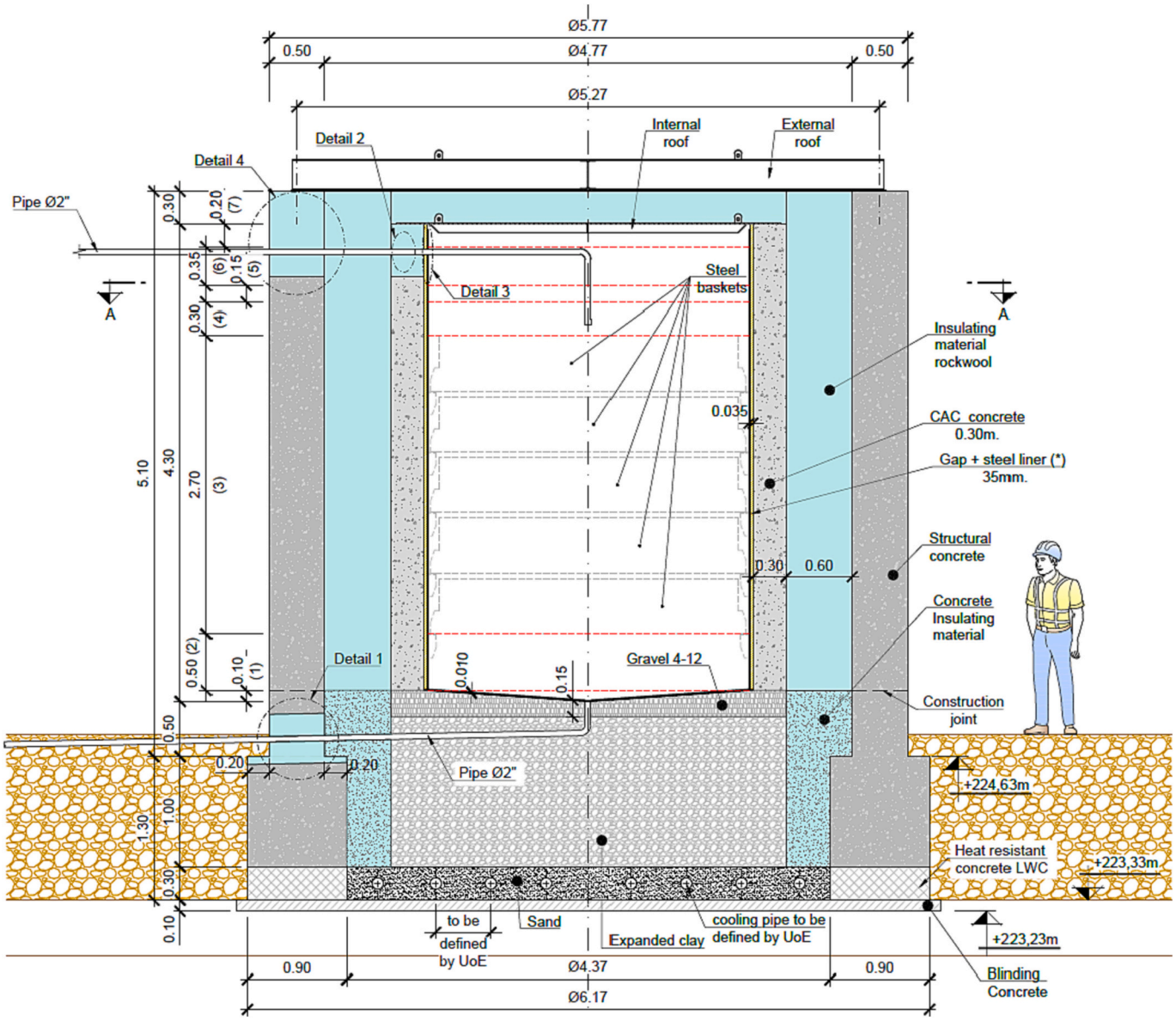

Fig. 1. Details of overall single tank designed for heat storage system.

2.3. *Concrete at high temperature*

In recent years some studies have considered concrete as an alternative low-cost sensible heat material for thermal energy storage [9] and it has been demonstrated its appropriateness for this application based on experiments at lab-scale exposing concrete to heat cycling [16,17,34] and the scale-up in modular prototypes with temperatures, up to 400 °C [35]. The use of concrete as part of the TES infrastructures, as in tank walls, needs to be suitable for being operated at high temperatures taking into account the temperature limits of the storage medium during cycling operation. Currently the operational and suitability of concrete for this role in TES application is not significant.

When concrete is exposed to high temperatures the material experience some physical and chemical changes [17,34,36–39]. During the heating process, up to 100 °C concrete loses first the free water that is located in the pores, above 100 °C most of the binding water in the hydrated solid phases is released, in a temperature region that depends on the cement type, for OPC-based cement between 100 and 500 °C and for CAC the dehydration of the solid phases mainly occurs up to 300 °C, as described in [17,34]. The generation of water vapour increases the pore pressure and, in combination with the internal thermal stresses occurring in the concrete, can undergo a spalling phenomenon with a collapse of the infrastructure [40–43]. In the case of concrete made of Calcium Aluminate Cement (CAC), as mentioned above when the temperature reaches 300 °C, the dehydration of the cement paste is mostly finished and the concrete is ready for its operation at high temperatures (up to 550 °C demonstrated) and under thermal cyclic regimes [17,34,44]. Henceforth, as the temperature of concrete increases, the variations in volume also take place due to the shrinkage of the cement paste and the heat expansion of aggregates [36,37,40].

Focussing on the tank-section, the preheating process of the CAC concrete layer of the wall of the tank is the most critical phase owing to the physical and chemical transformations that take place at these temperatures to allow concrete mechanical properties to stabilise [17,34]. For the above-mentioned reasons, the first preheating process in concrete TES infrastructure before the operation is crucial and decisive to its good operability as well as durability (thermal fatigue resistance).

Having this context in mind, the thermal exposure of the prototype section of the thermocline tank wall was made in cycling assuming the

temperature limits of operation of the selected molten salts.

The limits of the operating temperatures of the heat source of the thank-section were established at 200 °C and 500 °C to cover new advances in molten salt technology and to prove if such an energy storage system can be applied on a large scale to future concentrating solar power plants.

3. Thermocline prototype design

The conventional two-tank TES systems with molten salts existing in CSP Plants are tanks mainly made of stainless steel, as is shown in Fig. 2-left. The tanks are insulated with mineral wool to the environment to reduce the heat transfer losses and the whole storage infrastructure against storage media, which is characterised by having an elevated cost ratio [25,45]. The roofs are self-supported, and they are insulated with calcium silicate blocks to reduce energy losses. The foundations comprise different layers including a concrete slab, a thermal foundation refractory concrete insulation, a steel plate liner and sand [45].

The novelty of the TES system under investigation, developed under the NewSOL project was to prove the substitution of the stainless steel tank, 2.5–3 cm thickness on average [11], by a hybrid tank made of concrete with a thinner steel liner of 1cm of thickness to avoid the direct contact of the MS with the thermal concrete wall. For such an aim, the partial substitution of the thick steel liner by a high thermal performance concrete wall, able to withstand high temperatures and cyclic regimes, was designed and tested, as shown in Fig. 1. Whereas conventional tanks infrastructures are made of stainless steel and insulated as is shown in Fig. 2-left, the design of this hybrid thermocline tank concept (Fig. 2-right) comprises layers from the heat source to the external surface as follows: 1) a thin steel liner working as a container for the molten salts, 2) an air gap interface to allow the thermal expansions of the steel container during the operation as a consequence of the hydrostatic pressures generated by the hot molten salt, 3) a high thermal performance concrete able to withstand high temperatures under thermal cyclic operation, 4) insulating materials (rock wool for the top and walls of the tank and expanded clay in compacted sand bed for foundations) to minimize the heat transfer losses to the environment and 5) an external wall of reinforced concrete to support the whole TES system and allow to bear safely any the tensile forces of the hydrostatic pressure developed inside the tank walls during hot and thermal cycling.

The hybrid thermocline concept design (Fig. 2-right) has been defined in terms of materials and dimensions. The steel liner was the recommended solution for the thermocline concept design through experimental tests. as a result, the material considered for the steel liner is a Chrome Nickel Moly Alloyed Austenitic Stain Steel EN 1.4961,

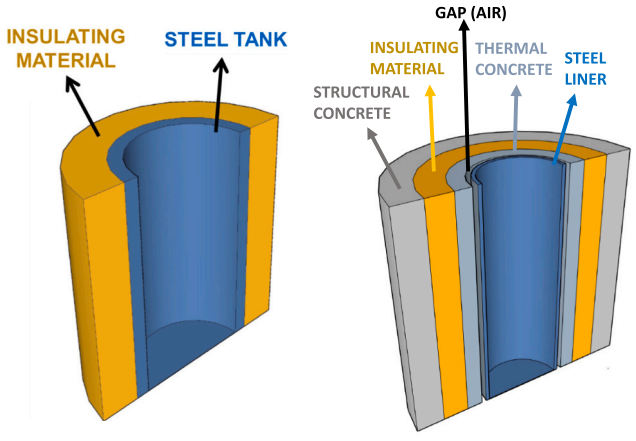

Fig. 2. Scheme of thermocline molten salts storage concepts: left) cross-section design of conventional steel-tanks walls and right) innovative hybrid steel liner/concrete tank wall.

equivalent to Stainless Steel AISI 321H, and 10 mm thick [46]. Besides the concrete layer composition and thermal conductivity were also selected according to previous experimental tests [34,38] to select the most appropriate concrete mix.

For the design of the thermocline tank, the analysis of structural and thermal calculations focused on tensile forces, heat losses and the temperature inside the wall distributed into the several layers of the tank, a finite element software (SAP2000) for structural analysis and simulation of vibration modes was used. This structural software has been proven as one of the most integrated engineering applications [47–49]. The structural calculations include several loads applied to the structure namely own weight as well as earthquake actions obtained as a result of the external and internal tensile forces on the concrete layers due to the hydrostatic pressure inside the tank from hot MS. Furthermore, the support and boundary conditions of the steel liner in the tank and the thermal properties of the molten salts were taken into account for the structural model. The air gap interface between the high thermal performance concrete and the steel tank liner was analysed in the structural model of an 8m height tank where both the Ultimate Limit State (ULS) and Serviceability Limit State (SLS) were verified. As a result, a maximum thickness of 25 mm air gap was estimated (at ambient temperature) to withstand any extreme thermal expansions of the steel liner tank filled with the molten salts during the operation at high temperatures. The air gap interface aims to allow the steel liner to adjust its position under the heat thermal expansion and the pressure of the MS reducing the risk of introducing high stresses in the storage system that could not be borne by the CAC concrete layer.

3.1. Thermocline tank section design for the assessment of the thermal performance

The prototype under investigation simulates a section of the hybrid-designed cylindrical thermocline tank concept. The performance at high temperatures of all the components in the section has been evaluated considering two stages: 1) during commissioning and 2) during operation considering charge/discharge thermal cycles, to analyse the feasibility for further up-scale applications: The monitoring of the evolution of thermal parameters with conventional thermocouple sensors located between the different layers across the section of the tank.

In this study, the prototype section investigated had the following total dimension of 1525 × 1700 × 1600 mm^3. As shown in Fig. 3, the section of the thermocline tank comprised different parts: 1) the section tank wall from the heat source to the external surface, 2) the top insulation, 3) insulation around the wall section and 4) the foundations at the bottom working as insulation as well.

The layers of the thermocline section wall comprised the following components: 1) heating mats (HHM and LHM) simulating the heat coming from the molten salts (dimensions of 457 × 457 mm), 2) a mild steel sheet plate, called “steel liner” (SL), working as a container for the molten salts with a thickness of 10 mm, 3) the presence of an air gap (AG), safety requirement from the structural tank model, as an interface between the steel liner and the concrete layer to withstand the effect of thermal stresses that would occur during operation as a consequence of the steel liner expansion and the pressure of the molten salts during its impact and during the heat charging period. The selected dimension of the AG in the prototype was 15 mm in width, in proportion to the scale of the tank-section dimensions proportional to the real tank size designed, shown in Fig. 1 and to a more efficient measurement of thermal changes along the AG during thermal cycling operation. 4) a high thermal performance concrete layer (CAC) with a volume of 300 × 500 × 1000 mm^3 able to withstand 550 °C and 5) an insulating (I) material of 600 mm of thickness to minimize the heat losses to the surroundings. The mentioned layers were located above an expanded clay with a sand-compacted bed of 250 mm in height and the whole system was isolated with rock wool to reduce heat losses to the environment. The top part of the prototype was insulated with 350 mm of

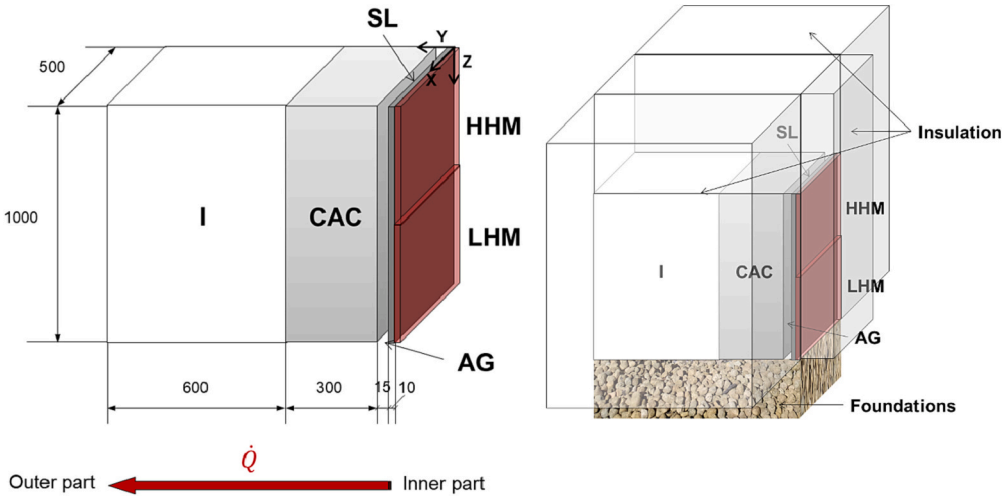

Fig. 3. left) Layers of the wall with dimensions and right) layers of the prototype of a thermocline tank section. The acronyms used for the Higher Heating Mat (HHM), Lower Heating Mat (LHM), steel liner (SL), air gap (AG), concrete layer (CAC), insulation (I) and foundations. The thermal power is expressed as $\dot{Q}$ [W].

insulating material (rock wool). Finally, the whole system was insulated around with a thickness of rock wool of 600 mm to minimize the heat transfer losses to the environment. The foundations were simulated using expanded clay with a sand-compacted bed to avoid thermal losses.

The schematic position of the layers of the tank-section, with the dimensions in millimetres, is shown in Fig. 3-left. Additionally, Fig. 3-right shows all of the layers involved in the thermocline tank section, including the wall, foundations and insulation around the prototype and the roof.

4. Experimental setup and methodology

4.1. Components of thermocline tank-section

Table 1 shows the materials and components involved in the layers of the prototype. The heat source was performed with two heating mats of flexible resistances covered with fibreglass and able to operate up to 500 °C. The steel liner was a mild steel sheet plate S275 JR, ferritic stainless steel with good behaviour under abrasion and corrosion, appropriate for being in contact with molten salts and at high temperatures [46]. The interface between the steel liner and concrete layer was simulated with a cavity of air at atmospheric pressure. Regarding the type of concrete, the selected concrete mix was the optimized solution found in [34], whose detailed concrete dosage is summarised in Table 2. The compressive strength of the concrete was tested after 7 days, achieving 48 ± 1 MPa. The insulating materials used were rock wool for the wall and top part of the tank-section, model TECH Slab HT 6.1, from Isover and for the foundations expanded clay with a sand compacted bed was used.

Table 1
Components of the thermocline tank section.

Layer		Dimensions	Characteristics
Wall	Heating mats (HHM & LHM)	457 × 457 mm	Flexible resistances covered with fibreglass Model: SXH-18 × 18–2-A, from Electrifor
	Steel liner (SL)	1000 × 500 × 10 mm	Mild steel sheet plate S275 JR
	Interface (AG)	1000 × 500 × 15 mm	Cavity with air at atm. pressure
	Concrete layer (CAC)	1000 × 500 × 300 mm	High thermal performance concrete
	An insulating layer (I)	1000 × 500 × 600 mm	Rock wool Model: TECH Slab HT 6.1, from Isover
Foundations		925 × 500 × 250 mm	Expanded clay with a sand-compacted bed
Insulation top		925 × 500 × 350 mm	Rock wool Model: TECH Slab HT 6.1, from Isover
Insulation around the wall		600 mm of thickness	Rock wool Model: TECH Slab HT 6.1, from Isover

4.2. Instrumentation of the thermocline tank section

The aim was to evaluate the thermal performance of the tank-section wall of the thermocline concept as well as to have effective monitoring references of the thermal performance to support the up-scale of the technology.

For this purpose, the whole system was instrumented with K-type thermocouples (nickel-chromium/nickel-alumel main composition, the most common type of thermocouples that are stable up to around 1.100 C). They were located between the layers of the prototype to record and quantify the temperature profile across the full section. The schematic position of the thermocouples placed between the different layers: IL 1 (on steel liner contact with heat mats and on external surface CAC concrete layer), IL 2 (from CAC external surface to rear CAC concrete layer), IL 3 (from rear CAC concrete layer to rear rock wool layer) is shown in Fig. 4. The coordinates concerning the location of the thermocouples (black points in 4) where the temperatures were recorded are shown in Table 3. Also, thermocouples were embedded in different depths and heights of the CAC layer, although not included in the present paper they have been considered in [38,51].

The execution of the test required a specific heating system, which consists of the following components: a controller, electrical heating mats and 6 Sensors Pt 100–500 °C to communicate the previous components. The model of the controller was Dual Loop Controller RE 92, an advanced dual loop controller designed to control two physical values in one object.

The heat source had a control system able to make the heating and cooling processes with a controlled time and heating rates. The accuracy of the programmed temperature of the heat source was ±2 °C. The measurements of temperature with the calibrated K-type thermocouples have an accuracy of ±0.1 °C. All temperature data collected by conventional thermocouples were recorded with a data acquisition system (Model: Agilent 34970A).

In summary, the test comprised of the following components: two heating mats, a controller, sensors Pt 100, a steel liner, a concrete layer,

Table 2
Composition of the high thermal performance concrete.

	Cement CAC	Water	Coarse aggregates (3–12 mm)	Fine aggregates (0–3 mm)	Polypropylene fibres	Plasticizer
kg/m^3	600	258	821	842	2	0.9

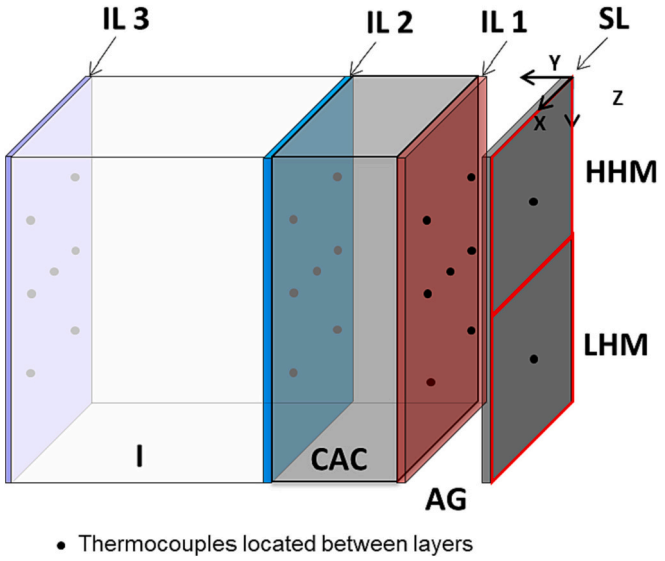

Fig. 4. Location of thermocouples on the surfaces of the different layers of the thermocline section.

Table 3
Coordinates of the thermocouples placed in the prototype. X, the width distance, Y, the length distance, from the heat source and Z, the height distance, in mm.

Location	Coordinates (mm)		
	X	Y	Z
HHM	250	0	250
LHM	250	0	750
IL1 (on SLmats surfaces + AG on external surface CAC layer)	120	25	250
			500
			750
	230	25	500
	400	25	250
			500
			750
IL2 (further external surface of CAC with insulation)	100	325	250
			500
			750
	270	325	500
	380	325	250
			500
			750
IL3 (further external surface of insulation)	100	925	250
			500
			750
	270	925	500
	380	925	250
			500
			750

an insulating layer, K-type thermocouples, a data acquisition system and a computer.

4.3. Final arrangement of the prototype

Table 4 shows some pictures taken during the positioning of the layers and the final arrangement of the prototype. Firstly, the foundation was prepared made with expanded clay having compacted sand. A wood frame was located on the foundation bed for the CAC concrete layer fabrication instrumented with embedded thermocouples. After hardening the wood frame was removed and then, some thermocouples were

Table 4
Pictures of section layers and final arrangement of the prototype.

Step 1: Fabrication of the concrete layer and location of the thermocouples on the surface and sand-clay compacted bed

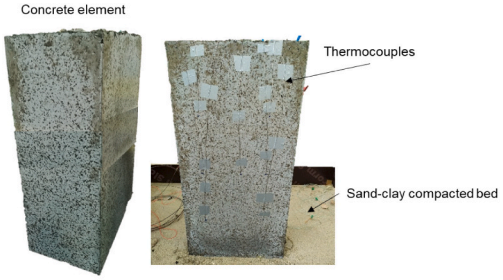

Step 2: Steel liner, air gap and insulation around the concrete layer

Frontal view

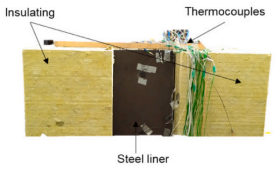

View from the top

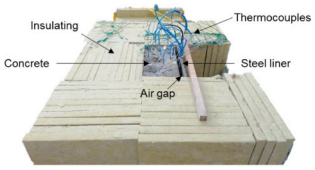

Step 3: Insulation of the top of the concrete

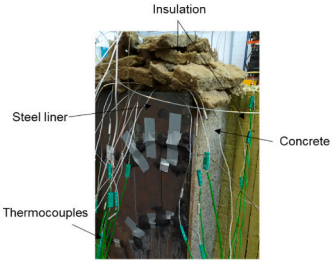

Step 4: Location of the heating mats

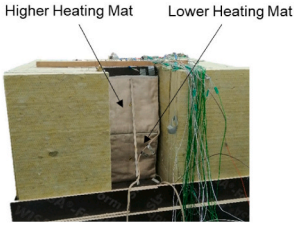

Step 5: Final arrangement of the prototype

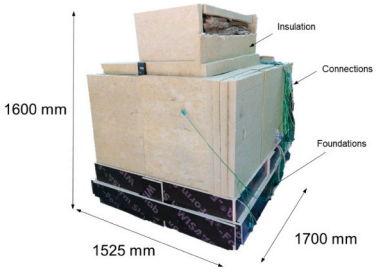

located in the interface layers of the thermocline section to record and quantify the temperature profile across the full section. The details of the sand-clay compacted bed and the location of thermocouples on the surface of the concrete are shown in step 1 from Table 4. After that, the insulation was placed around the concrete layer as well as the steel liner, maintaining the air gap between them (step 2). Once the connections were done accordingly and verified, the top of the concrete layer was insulated, as is reflected in step 3. The following step was to place the heating mats in the correct place in contact with the steel liner (step 4). Finally, the whole system was thermally isolated to reduce heat losses to the environment. The final disposition of the prototype section of the thermocline tank is shown in step 5.

4.4. Thermal regime for the operation of the tank-section

Before starting with the operation of the tank section (cyclic heat charge/discharge), the prototype was commissioned. The infrastructure was preconditioned with a preheating process up to 300 °C by slowly heating in steps to allow the dehydration and loss of moisture of the concrete and reduce the risk of spalling during the operation charge/discharge at high temperatures. Firstly, the temperature increased up to 100 °C for 24 h to allow for the loss of free water from concrete and the drying process. After that, to produce the dehydration of the cement paste of the CAC concrete, two plateaus of constant temperature at 200 and 300 °C were established to make the temperature homogeneous and to avoid high thermal gradients within the concrete layer. The temperature at those plateaus was maintained for 24 h. After the whole system was preconditioned (commissioning), a thermal cycling regime for the operation of the thermocline section was designed following recommendations in previous studies [34,37,38].

4.4.1. Thermal cycling curve for the operation of the tank-section

Three full charge/discharge cycles were performed to assess the operation phase of the tank section. The heating and cooling cycles lasted 75 h and a cooling process down to room temperature. The thermal cycling test stage covered the heating and cooling cycles between 200 and 500 °C, as shown in Fig. 5, to simulate the operation of a thermocline tank to analyse the evolution of the thermocline volume. As the test was carried out with two heating mats with two control systems, they were operated at different temperatures and heat time was delayed. The plateaus of temperature were maintained for 4 h to achieve 1 daily charge cycle. The first heating up to the maximum temperature (500 °C) was made to achieve 300 °C in the air chamber. Regarding the cooling process, it followed a natural draft.

The charging and discharging process of the thermocline tank section was induced in the prototype through two heating mats, as shown in Fig. 6. Three different processes have been identified. The initial state is the end of the drying and dehydration curve when the heat source was at

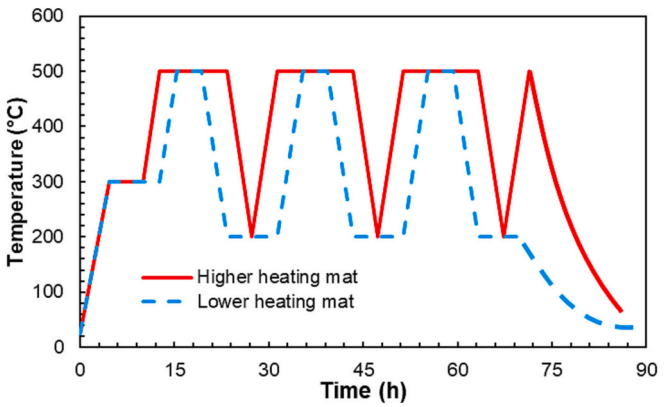

Fig. 5. Thermal cycling curve.

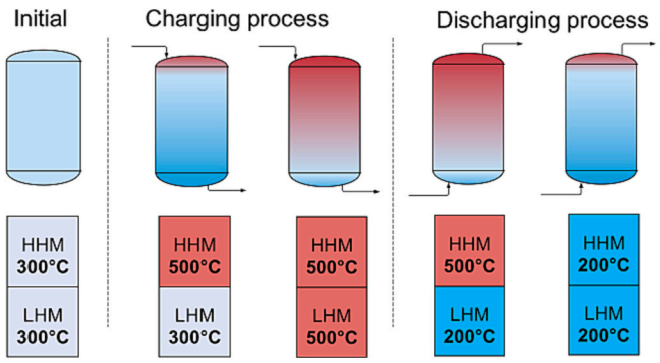

Fig. 6. Simulated thermal cycling process operation of the prototype in the heating mats.

300 °C. The charging process starts from the top and the heated molten salts come into the tank from the upper part and the cold ones go out of the tank from the bottom. Therefore, the Higher Heating Mat (HHM) was heated up to 500 °C while the Lower Heating Mat (LHM) remained constant. After that, the LHM was heated up to 500 °C to simulate a thermocline fully charged. It remained at the maximum temperature for 4 h and then the discharging process was simulated. The discharge is produced backwards, and the heated molten salts go out of the tank from the top and the cold salts come into the tank from the bottom. Given this process, firstly the LHM was cooled down to 200 °C and then the HHM was cooled down to the minimum temperature. Once both heating sources were at 200 °C the thermal curve was repeated to simulate the thermal cycling stage.

The output parameters measured with conventional thermocouples during the test were the temperature across all layers of the prototype at 3 heights (250, 500 and 750 mm) and were recorded every 5 min.

5. Results

5.1. Evolution of temperatures across the tank section during commissioning

A commissioning stage in the case of the hybrid thermocline concept was considered. Its relevance is based on two reasons: 1) verification of the heat performance of all components constituting the tank section and 2) the preconditioning of the concrete layer to reduce the free and bound water content that could cause any risk of spalling during the operation process.

The whole process lasted 75 h, including the three heating steps. Different aspects were appreciated, as shown in Fig. 7: the presence of the air-gap favour the formation of a decreased gradient of temperature between the steel liner and the CAC concrete layer. The heating of the air in the air gap, that is the temperature at the surface of the concrete layer, has allowed a progressive drying of the concrete to occur, temperatures between 100 and 175 °C were measured at the surface of the other end of the concrete layer after the 75 h heating of the commissioning. The rock wool and foundations have shown a good isolating capacity. The cooling process shows a rapid decay of temperature of the heat mat and the air gap, while a gradient of temperature decay is appreciated in the concrete indicating the inertia to heat losses of this material.

5.2. Evolution of temperatures across the tank section during cycling operation

A first preheating of the system was made to achieve a temperature of 300 °C in the air gap to simulate the condition after the commissioning/preheating process. Once the air gap reached the target temperature, the first heat (charge) cycle started and the heating process up to 500 °C was made according to the heating regime described in Figs. 5

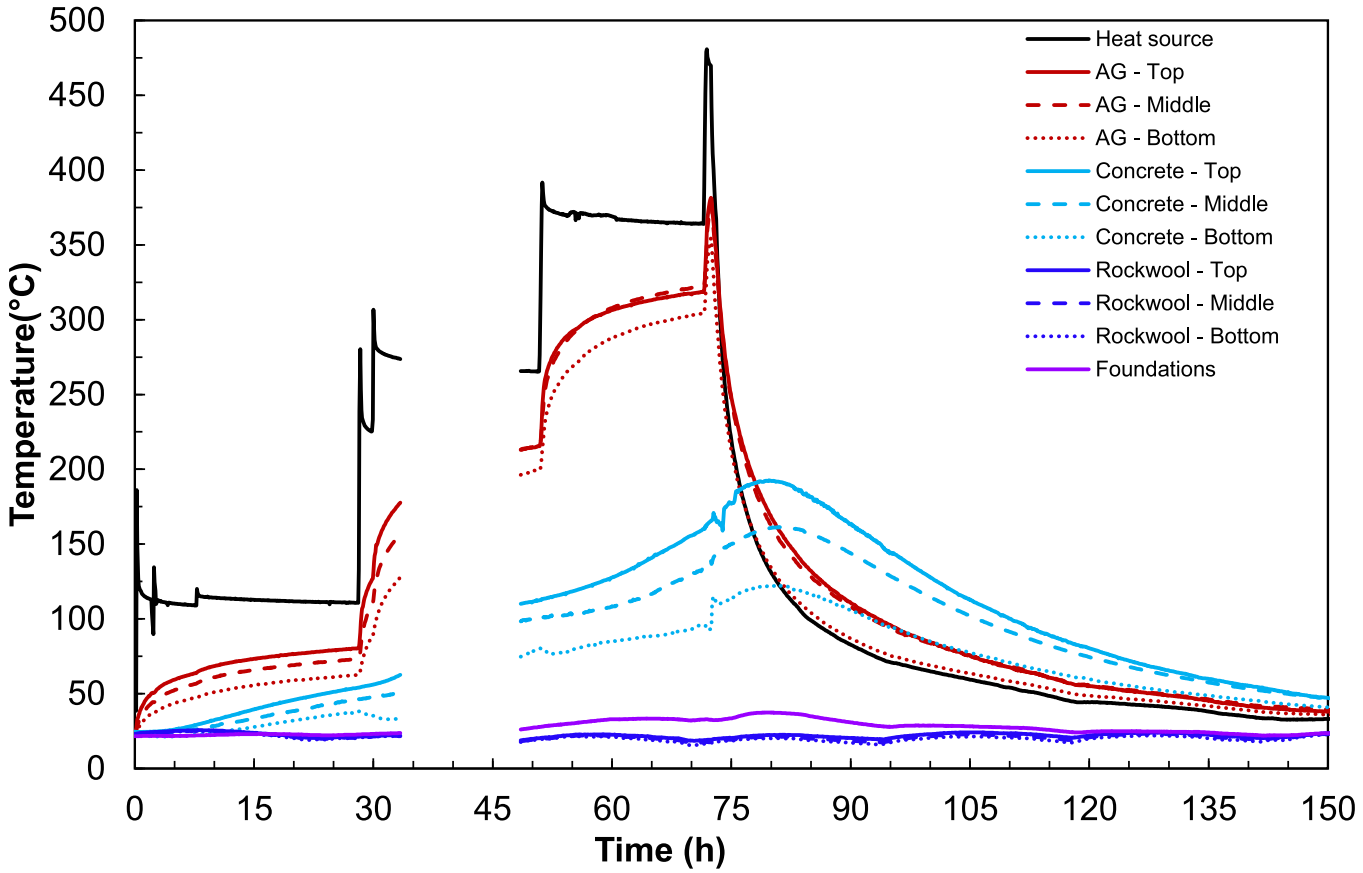

Fig. 7. Evolution of temperature across the tank section layers during commissioning.

and 6.

Fig. 8 shows the evolution of temperature during the test across all the layers of the tank section. The interface temperatures of the layers are differentiated in colour, in black for the heating source (heating mats), in red for the air gap at the surface of the CAC layer closer to the heat source, in light blue for the other end of the CAC layer (rear concrete surface), in dark blue for the end of the insulating layer and violet for the recorded temperatures at the bottom of the prototype

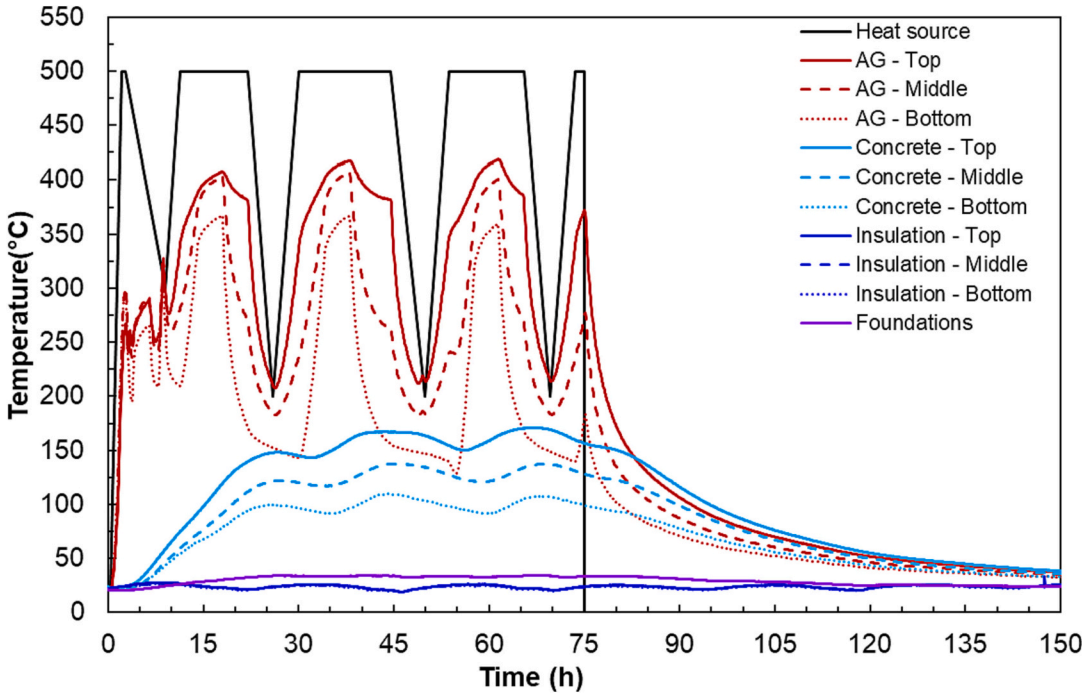

Fig. 8. Evolution of temperature across the layers of the tank section.

(foundation). The temperatures recorded at the top (250 mm), middle (500 mm) and bottom (750 mm) are represented with a continuous line, a dashed line and a dotted line, respectively following the same colour distribution for each layer at the middle and bottom level. No significant differences in the X direction of the tank section for each height were found, so the values of the mean temperature were considered to simplify and highlight the temperature differences in height and width (Y and Z as indicated in Fig. 4 and Table 3).

The gradient of temperature response of each layer is repeated in the three cycles and across the length of the tank section. There is observed a gradient of temperature in the air gap, with also a gradient in the height (Z direction of the tank section). These gradients of temperature are also appreciated at the rear surface of the concrete layer, between 100 and 150 °C. The good isolation response of the Rockwool and foundation is appreciated and kept around 25 °C during the charge/discharge cycles.

The temperature differences across the layers are represented in Fig. 9 for each cycling step as follows: i) the first heating up to reach 300 °C in the air gap (initial condition before starting with the charge/discharge operation cycling of the thermocline section, time = 3 h), and the ii) maximum and iii) minimum operating temperatures of each cycle when the heat source was at 500 °C (time = 40 h) and 200 °C (time = 50 h), respectively.

The results of the thermal cycling stage highlighted the following issues that are of interest to understanding the thermal performance of the thermocline hybrid tank concept:

1) Air gap interface (AG): The role of the air gap was notable. It is remarkable the "air gap effect" acts as a chimney because the highest temperature difference took place between the steel liner and the surface of the CAC concrete layer. Those values were above 200 °C whereas the top achieved a maximum ΔT of 175 °C at the beginning of the heating when the AG was heated to achieve 300 °C before performing the thermal cycles from 200 to 500 °C. When the heat source was set at 500 °C, the CAC surface was at 420 °C at the top and 375 °C at the bottom. For the minimum temperature of the cycles (200 °C), the temperature differences were slightly lower due to the thermal inertia during the cooling process. Moreover, a convection heat transfer mechanism takes place in the air gap interface, being detected by the thermocouples located at 500 mm at different heights. This is justified by a convection heat flow from the bottom to the top of the air gap interface of the tank section facilitating heat decrease from the liner of the tank to the surroundings during the discharge process.

It is worth noting that a hybrid thermocline tank concept having an air gap interface is a relevant part of the heat energy stored and contributes to the charge/discharge process. In the hybrid thermocline design concept, as discussed in 3, the air gap was considered to ensure the structural stability of the tank infrastructure regarding the thermal expansions and internal hydrostatic pressures from the molten salt heating during the operation of the thermocline. The boundary conditions of the section of the tank tested allowed displacements because the movements were not restricted. In a real tank, the thickness of the air gap could vary during operation because of the thermal expansion of the steel liner and pressures of the heated molten salts. This fact would reduce the volume of the air gap interface, in the tank-section dimension, a lower thickness of the air gap with respect to the maximum size calculated in the structural model was considered and heat convection was observed within the air chamber. Very likely, the effect related to convection in the air gap would be significantly reduced if the air gap width also decreases during the operation of the thermocline. Assuming that the air gap dimension will vary along the charge/discharge of each heat cycle the presence of the air gap influence for the hybrid thermocline concept has to be taken into account. The experimental results of the present study have been useful for the design and calculations of an upscale thermocline tank with a cylindrical shape of 8 m height that has been designed, as shown in Fig. 1, built in NEWSOL project.

2) Thermal concrete layer (CAC): the maximum temperature achieved in the concrete tested was between 425 and 350 °C and the temperature difference within the material (ΔT_{CAC}) was 250 °C. The type of concrete used for the CAC layer has been demonstrated to have high thermal resistance up to temperatures of 550 °C described [34]. Despite undergoing such high-temperature difference, the CAC concrete layer withstood the cycling properly and its use as both a structural and insulating layer was proven. The effect of heat cycles on the mechanical properties of the concrete layer was measured in cores taken at different heights and depths of the CAC layer, results not being part of the present paper, compressive strength reductions were found between 15 and 35 % [51] after 3 heat cycles, significantly lower than the limit measured in small concrete samples [34]. The residual strength of this high thermal concrete after 75 heat cycles reaching the equilibrium at 550 °C in the sample remains stabilised at 37 % [34]. A fatigue analyses considering the evolution of the mechanical properties after operation of the tank-section and the compressive strength measured in [34] after 75 heat cycles and the prediction for daily thermal cycles up to analysing the long-term

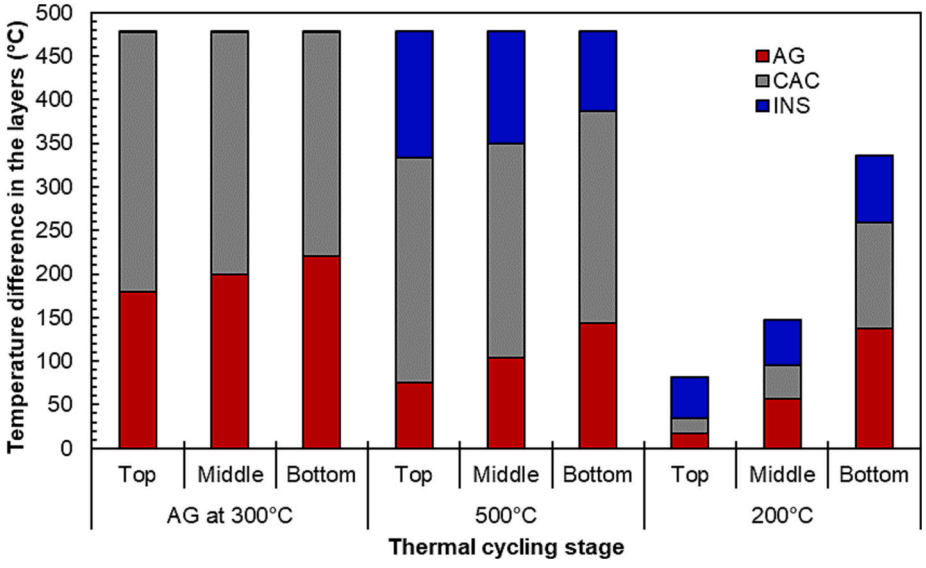

Fig. 9. Temperature differences in the layers of the prototype.

stability (a lifetime of 25 years) suggested the suitability of using the hybrid thermocline design concept in CSP plants.

3) Insulation (I): The operation at the maximum temperature during the cycles did not increase the temperature at the external part of the insulation. For that reason, the thickness of insulation in combination with the high thermal performance concrete has been demonstrated as a utility arrangement for avoiding damage to the TES infrastructure, which would maintain its mechanical properties without compromising the tank infrastructure. Regarding the difference in temperatures, they were similar when the prototype was being operated both at 200 °C and 500 °C.
4) Foundations: The thermocouples located in the sand-clay compacted bed did not register temperatures above 40 °C. Owing to this fact, the heat transfer losses from the prototype to the soil were minimal compared to other layers (steel liner, air gap and CAC). This was an important finding of this investigation.

Furthermore, two temperature profiles within the layers were shown: i) when the thermal cycle was at 500 °C (time = 40 h) and ii) when the thermal cycle was at 200 °C (time = 50 h). The evolution of the temperature across the prototype from the heat source to the end of the insulation when the heat source was at 500 °C and 200 °C is shown in Fig. 10. The temperature experienced the biggest drop across the concrete layer when the prototype was operating at the maximum temperature. Comparing different heights, the top and middle parts followed a similar response in the concrete, but the convection effect of the air gap (chimney action) was predominant at the top. The concrete temperature decreases faster at the top and of the thermocline tank in contact with the air gap. For that reason, regions closer to the air gap reduced their temperature faster than the further ones, and this explains why the top and middle remained almost constant along with the distance of the concrete. Although during heat charge the air gap interface works as an isolator for the concrete while during the heat discharge the presence of the heated concrete helps to keep the temperature in the air gap at a level to prevent the freezing of the molten salts. In the extreme operating condition of the air gap interface volume close to cero, the CAC wall layer could reach the maximum temperature (500 °C in the present case) that the concrete layer is expected to withstand due to the specific high thermal performance considered in the concrete design [34]. Besides the concept of the thermocline tank designed, as described in Figs. 1 and 2-right, the external wall of the reinforced concrete will support the whole TES system and allow it to bear safely any extra tensile forces of the hydrostatic pressure developed inside the tank walls during long-term hot and thermal cycling.

5.3. *Thermal response of the tank section in charge-discharge operation cycles*

A deep analysis of the thermal response of the tank section was carried out following the evolution of the profiles of temperature to see the distribution of heat along the system during the test. For such an aim, a MATLAB® routine was developed to interpolate the temperatures

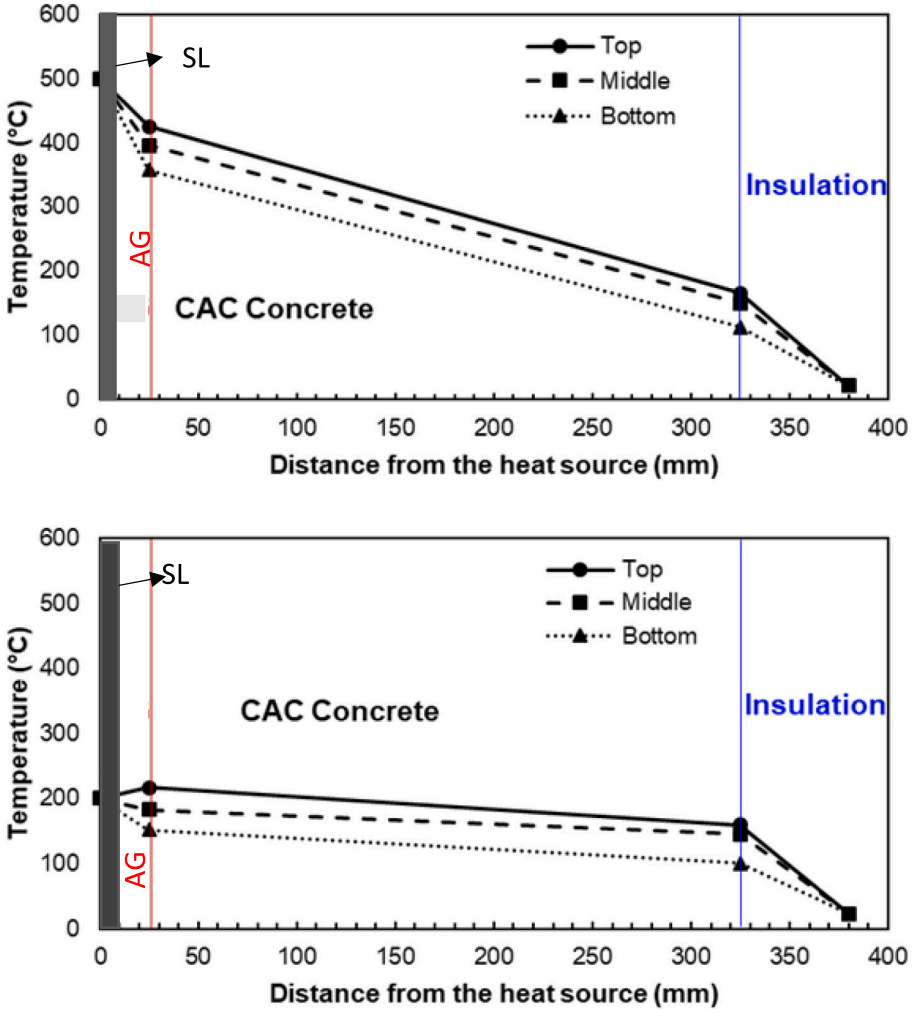

Fig. 10. Evolution of temperature along with the heat source operating at 500 °C (top) and 200 °C (bottom) during the cycling.

known in those nodes where the thermocouples were located in the prototype to obtain the 3D temperature colour map in the whole prototype [50]. The MATLAB® code applies an interpolant linear function to determine the temperature in the whole section. The section of the tank has been simulated with a mesh of the same dimensions as the real prototype and the coordinates X, Y and Z and the axes represented in the simulation follow the same coordinate system as the diagram shown in Fig. 4 and Table 3. The code was run for obtaining the 3D temperature colour map across the tank section. As this only reflects 3 planes, more representations were done to reflect the temperature in slices at chosen locations. Firstly, the global 3D of the prototype with slices at positions X = [0, −500] mm, Y = [0, 925] mm and Z = [0, −1000] mm. Secondly, slices in plane Y were chosen to obtain the evolution of temperatures for the heat source. The selected slices in plane Y were: 0, 25, 85, 185, 270, 325, and 925 mm, related to the surfaces of the air gap, the first concrete surface, and the thermocouples embedded into the concrete at 85–185–270 mm, although the temperature data are not included in the present paper, however, data have been considered for the interpolation [51], interface layer between CAC concrete and Rockwool (350 mm) and the end of the Rockwool (925 mm). After that, the code was run for planes at different heights that were chosen according to the position of thermocouples in Z axes: 0, −250, −500, −750 and −1000 mm from the top. Finally, some X-planes were represented as well (X = 100, 120, 230, 270, 380 and 500 mm) to evaluate the temperature profiles across the longitudinal section of the prototype.

5.3.1. Case studies

The test results in terms of temperature profiles might be obtained for the entire testing time. However, as the temperature profiles changed every 5 min, the pictures shown in this investigation attain representative case studies chosen for different thermal cycling conditions, as shown in Table 5. To ensure steady-state conditions, the case studies were investigated once the system had achieved equilibrium. Case study (CS) 1 represented the starting conditions (commissioning process) before starting the cycling. CS 2 is related to the condition when both heating mats were at 500 °C in the first thermal cycle. CS 3 shows the case when both heating mats were at 200 °C. Regarding thermal cycling, CS 4 and 6 are associated with the operation at 500 °C at the 2nd and 3rd cycle, respectively. In contrast, CS 5 and 7 correspond to the operation at 200 °C at the 2nd and 3rd cycle, respectively.

The evolution of the temperature colour map in the prototype is shown in different isometric images included in Table 6. All pictures were labelled as 'Width', 'Length' and 'Height' corresponding to the axes X, Y and Z, respectively. Table 6 includes the isometric perspective and the 3D temperature colour map of the whole prototype, whose external surfaces were represented. The temperature was represented in form of a colour bar, from dark blue at 20 °C to red at 500 °C.

Analysing the profiles of CS 2, 4 and 6, the evolution of temperatures in the external surfaces was almost similar because the heat source was operating at the maximum temperature (both heating mats at 500 °C). Despite the tank section being exposed to the maximum temperature, the heat did not arrive at the end of the concrete layer. Indeed, this layer was the one that underwent the highest variation of colour, meaning that the concrete layer acted as an insulating material and this was an important finding of this investigation.

Table 5
Case studies for the simulations and the thermal model.

Case study	The temperature of the heat source	Cumulative time [h]
1	300 °C	8.66
2	500 °C, 1st cycle	17.92
3	200 °C, 1st cycle	30.00
4	500 °C, 2nd cycle	38.00
5	200 °C, 2nd cycle	50.00
6	500 °C, 3rd cycle	61.58
7	200 °C, 3rd cycle	71.33

On the other hand, it is worth noting the effect of the thermocline that can be observed in CS 3, where the top was at a higher temperature than the bottom. This condition generated a 'corner effect' which is visible in the image taken 30 h after the start of the test. Another point of interest is when the heat source was at the minimum temperature of cycling (200 °C) as in CS 5 and 7, where the temperature was a little bit higher at the top. The explanation for this was the thermal inertia and the heat transfer from the whole system to the environment. Due to the air gap effect, the heat transfer was bigger at the top of the air gap chamber, suggesting the need for good isolation at the roof of the thermocline tank is needed. This is the reason why the temperature was higher in regions closer to the heat source and in the upper part. It is important to highlight that the conditions tested referred to the scenario with the air gap interface, in the present study considering that it does not suffer a volume change during the charge state of the thermocline and maintains the width during the operation of the thermocline, increasing the convection and heat transfer process. This situation allows also to notice that the three repetitive cycles of charge and discharge show similar profiles of temperatures.

On the other hand, in all CS, the temperature reached the maximum at the centre of the layer and the thermal parameter decreased when the location was closer to the corners. Although the heat transfer changes were lower, the energy decay resulted in a temperature decrease in those regions.

6. Discussion

The dimensions and geometry of the hybrid thermocline section allow the analyses of the performance of the different layers of the thermocline. Additionally, the discussion includes a list of pros and cons of the thermocline concept for its further implementation in an up-scaled industrial infrastructure as well as its differences from the two-tank TES system.

6.1. Lessons learned and recommendations from the operation of the prototype

6.1.1. Commissioning of the tank before filling with molten salts: pre-heating

The commissioning of a hybrid thermocline tank should include a preheating process before the cycling operation. Several technical reasons have to be considered: 1) to minimise the risk of MS freezing when entering a cool tank as also suggested in [52] due to the high freezing point, 234 °C for Solar Salt, 2) to allow the concrete layer drying and cement paste dehydration to stabilise the system, as suggested in [17,34] and to avoid any spalling risk, and 3) to reduce tank risks such as thermal gradient shocks in the layers or in the packed bed system that could induce high internal pressures, which could lead to mechanical performance reduction or critical structural failures, also avoiding the freezing of the salts. This is a critical and sensitive commissioning operation that must be taken into account.

Moreover, the temperature of the pre-heating process (commissioning) has to be chosen accordingly to the constructive layer configuration, material limits and the freezing point of the salt melted in the tank. In this study, the first heating of the empty thermocline tank was carried out up to 350 °C for achieving 300 °C in the air gap and the surface of the concrete layer. As the commonly-used Solar Salts typically operate with a cold temperature of 290 °C [4,52,53], this temperature has been selected as the minimum safe operation molten salt temperature. Nevertheless, other salts with a reduced melting point, such as a ternary mix patented [33] allow to work with lower temperatures and in this case, the pre-heating can be done at a lower temperature. For this ternary mix, the minimum safe operating temperature is 170 °C and, therefore, the pre-heating of the tank before filling it with salts could be done at a lower temperature (180–200 °C). That is the reason why this preheating temperature should be set depending on the materials

Table 6
Temperature profile of the tank section along the case studies investigated.

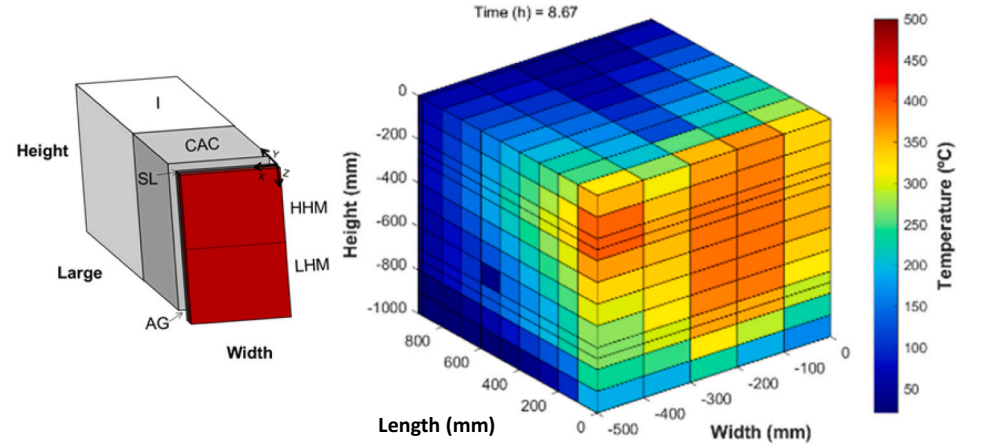

Case study 2

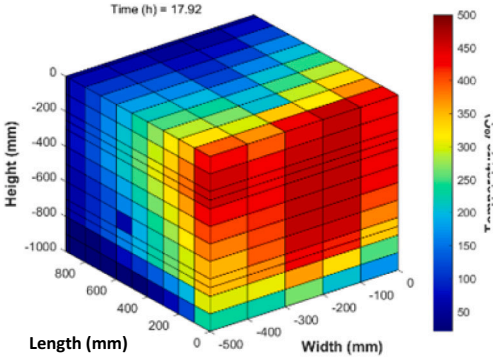

Case study 3

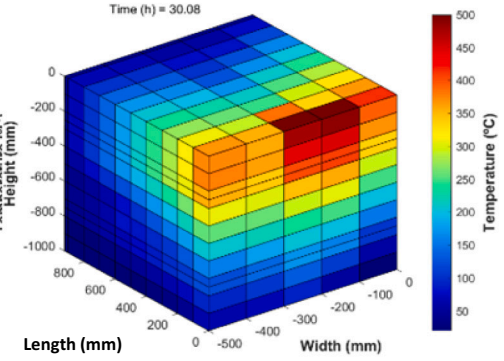

Case study 4

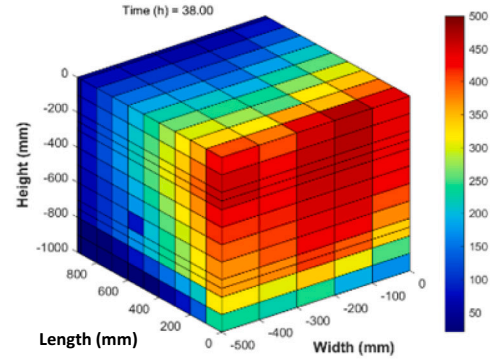

Case study 5

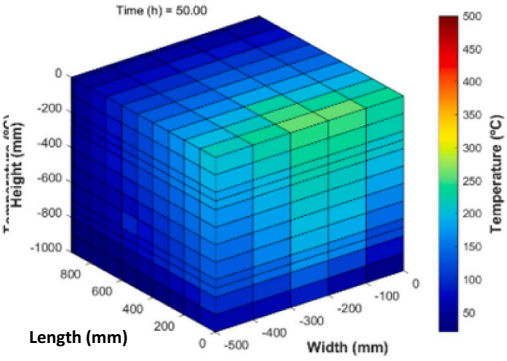

Case study 6

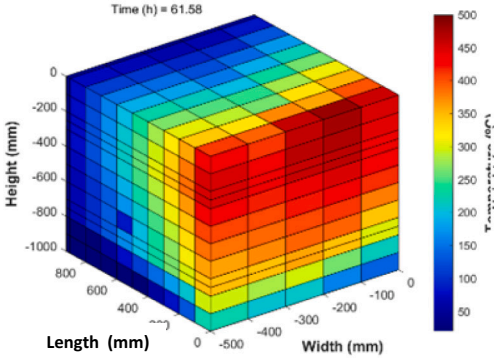

Case study 7

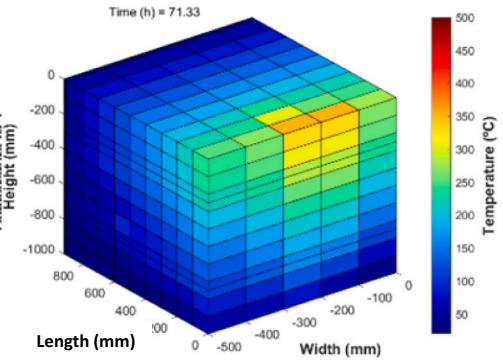

involved in the TES infrastructure.

6.1.2. The concept of a hybrid thermocline tank with a concrete layer demonstrated

The operation of the thermocline for the heating and cooling cycles has highlighted the thermal inertia of the system. The highest decrease in temperature was found in the concrete. The CAC concrete element has been able to withstand accurately the cyclic operation under high-temperature regimes.

Although the cooling process shows a rapid decay of temperature at the steel liner and in the air gap interface, the inertia of the concrete layer (to decrease the heat becomes a new heat source that allows maintaining such a level of temperature that reduces the risk of freezing of the molten salts in the tank.

Progress on using concrete as a structural thermal energy storage material was also reported by many authors at the lab scale [16,17,35]. Nevertheless, in this study, the novel concept of using concrete also as an insulating layer for tanks containing molten salts has been demonstrated. The higher thermal inertia of the concrete concerning the steel contributes to keeping the heat for longer in the region of the air gap, as can be deduced from Fig. 11 in the discharge cycle, reducing MS freeze. This beneficial effect of the heat inertia of the concrete layer could also permit a reduction of the dimensions of the insulation layer of Rockwool for conventional storage systems [11].

6.1.3. Design and operation of the hybrid thermocline tank

The analysis of the evolution of temperatures across the prototype highlighted the remarkable effect of the air gap chamber on the heat transfer process. It is worth noting that this layer has only a thickness of 0.015 m and the temperature difference experienced in the air gap chamber had a not negligible impact on the performance of the whole system. Indeed, it affects the closer layers of the infrastructure, which experience a heating process from the top and a cooling process at the bottom. The 'corner effect' produced differences in temperature in both longitudinal and transverse directions. In short, the air gap interface is necessary for the thermal expansions during operation, its presence also influences the local heat energy gradients that have to be considered with the good isolation at the roof of the thermocline. Nevertheless, the convection effects during the operation registered in the prototype referred to the scenario with the thickness of the air gap interface size maintained fixed. Although in the real thermocline operation the air gap can change in width between heat charge and discharge it is more conservative to consider its presence due to the structural requirement that the air gap absorbed the internal pressures and maintain the integrity of the whole TES system.

6.2. Limitations of the thermocline concept

It is important to note that the air gap experienced differences in temperatures between the top and bottom owing to the convection heat flow (chimney). Heat tends to go up and that is the reason why the temperature recorded at the top was always above 50 °C higher than the one recorded 500 mm below, as shown in Fig. 11. This outcome was found in just 500 mm of height, so the effect might be even higher in real thermocline tank sizes whose height would be bigger than 12 m and even reach 20 m, from simulations carried out [6,54,55].

The convection heat flow favours the heat transfer in the air gap which will affect the thermocline tank operation. Nonetheless, the air gap is needed from a mechanical safety point of view because the tank filled with molten salts will expand during the operation due to hydrostatic pressures. As a consequence, a balance between the geometry and the thermal operation of the infrastructure must be found in the following design steps.

The effect of the air gap might be reduced with a redesign of the air chamber to minimize the convective heat flow and, thus, the discharge of energy from the bottom to the top of the tank and good isolation at the top of the tank. Some baffles might be included in the geometry to change the direction of the airflow and avoid the generation of convection currents. Nevertheless, the baffles should be made of a material resistant to high temperatures and able to withstand changes in the volume of the steel tank due to thermal expansion. Optimization between the geometry and thermal operation of the tank must be found to increase efficiency so that the advantages arise when compared with the established two-tank system approach.

6.3. Comparison between thermocline and the two-tank concept

Configurations of energy storage can be compared in different terms attending to the global performance of each system. Some parameters are typically used for comparing electrical batteries such as the depth of discharge (DOD), which is the ratio between the thermal energy discharged to the maximum amount of energy that can be stored [56–58]. The DOD can also be applied to thermal energy storage configurations and, thus, to thermoclines or two tanks of molten salts, where DOD values are around 95–99% versus electric batteries where at most the DOD can be found between 70 and 80%. The thermocline region, where the temperature drop is located, causes exergy losses due to the contact of two fluids at different temperatures. Narrower thermocline regions produce lower exergy losses, as was reported by [10,59,60]. Nonetheless, despite the energy stored, those exergy losses cause the thermocline tanks to discharge lower energy compared to the two-tank technology, which does not present exergy losses because it has no temperature difference, and the efficiency is higher [9,11].

Another limitation of the thermocline tanks compared to the two tanks is the maximum outlet temperature of the fluid during the discharging process, named cut-off temperature. This temperature is not the maximum reached in the TES and during this process, the temperature of the fluid is not constant. For that reason, the roundtrip

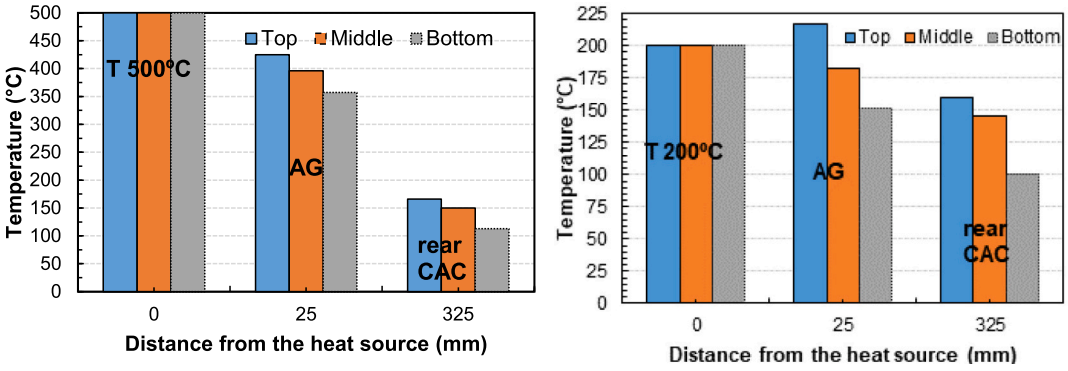

Fig. 11. Temperature at the layer surface at the end of charge and discharge cycle.

efficiency in the conversion from thermal to electrical in the power block is somewhat reduced.

On the other hand, the present prototype operation has arisen the issue of the thermal gradients due to the convection process within the air gap interface. If an air chamber was used as a layer in new thermocline systems, this would induce an increase in the auto-discharge ratio, which would be higher in the thermocline versus the two-tank system.

In terms of costs, building one thermocline instead of a two tank system (each with their own submersible pump), represents savings on CAPEX. The steel used in this hybrid steel & concrete thermocline tank is about 30% of the usual amount of steel for one tank with the same size.

Overall, this represents a cost advantage because of: 1 – to build one tank instead of two, 2 – 70% less steel for the hybrid tank and 3 – to save one submersible pump. Because of the beneficial enhancement of the temperature stratification inside a thermocline tank, the height versus diameter ratio shall be bigger on a thermocline tank, leading to higher tanks with corresponding higher amplitudes of its vibration modes, an item which can be relevant for regions with high earthquake risk.

Moreover, the proposed concrete structure would be beneficial for the two-tank TES system in the sense that a significant amount of steel would be saved, thus for the markets where concrete is a much more economical solution when compared to steel, it represents an important advantage.

7. Conclusions

In this paper, an experimental analysis of the thermal performance of a section prototype for its operation as a thermocline tank having and hybrid design concept of a thin steel liner and high thermal thick concrete layer and an air gap interface in between is considered. The evolution of the thermal response of different layers constituting the TES system subjected to a heat source ranging from 200 to 500 °C was investigated. The performance during the commissioning and operation of the prototype exposed to high temperatures has been analysed. Based on the experimental results presented in this work, the following conclusions can be drawn:

- A pre-heating process of the hybrid thermocline steel liner-concrete section during the commissioning has allowed verifying the correct functioning of each layer component of the section. Besides the preconditioning allows the concrete layer to reach temperature levels for free and bound water reduction.
- The CAC concrete layer has been able to withstand gradients of temperature in the length and height during the cyclic operation under regimes of high temperatures up to 425 °C.
- The high thermal concrete layer has acted as a suitable insulating and heat storage material, succeeding to withstand the thermal load during the cycles.
- The CAPEX cost of a thermocline tank is lower compared with the 2 tank system, the exact value depends on how big is the storage system
- The insulation layer of the Rockwool after the concrete layer and the expanded clay in the foundations experienced temperatures below 40 °C, reducing heat transfer losses to the exterior.
- The air gap interface generated a heat convection current that favours temperature gradients during heat cycling that allow energy loss but also the heat inertia inside contributes to avoiding freezing of the MS during the discharge process

CRediT authorship contribution statement

T. Lucio-Martin: Conceptualization, Investigation, Resources, Methodology, Data curation, Validation, Visualization, Writing – original draft, Writing – review & editing. **M. Martin:** Conceptualization, Investigation, Supervision. **L. Guerreiro:** Conceptualization, Investigation, Methodology, Writing – review & editing. **R.S. Villardón:** Conceptualization, Investigation, Resources, Methodology, Writing – original draft, Writing – review & editing. **J. Lopez:** Conceptualization, Investigation, Writing – original draft, Writing – review & editing. **M.C. Alonso:** Conceptualization, Investigation, Funding acquisition, Supervision, Writing – original draft, Writing – review & editing.

Declaration of competing interest

The authors declare the following financial interests/personal relationships which may be considered as potential competing interests: Maria Cruz Alonso reports a relationship with Spanish Scientific Research Council that includes: funding grants.

Data availability

No data was used for the research described in the article.

Acknowledgments

This investigation was carried out in the context of the NewSOL project, *New StOrage Latent and sensible concept for highly efficient CSP Plants*, and has received funding from the European Union's Horizon 2020 research and innovation programme under grant agreement No 720985. The authors would also like to thank *Cement Molins* for providing CAC and CAT and for the technical discussions.

References

[1] Y.-S. Chuang, H.-P. Cheng, Ch.-Ch. Cheng, The current development of the energy storage industry in Taiwan: A snapshot, J. Energy Storage 53 (2022), 105117, https://doi.org/10.1016/j.est.2022.105117.
[2] A. Gil, M. Medrano, I. Martorell, A. Lázaro, P. Dolado, B. Zalba, L.F. Cabeza, State of the art on high temperature thermal energy storage for power generation. Part 1—Concepts, materials and modelization, Renew. Sust. Energ. Rev. 14 (1) (2010) 31–55, https://doi.org/10.1016/j.rser.2009.07.035.
[3] V.A. Sötz, A. Bonk, J. Forstner, T. Bauer, Molten salt chemistry in nitrate salt storage systems: linking experiments and modelling, Energy Procedia 155 (2018) 503–513, https://doi.org/10.1016/j.egypro.2018.11.030.
[4] S. Ushak, A.G. Fernández, M. Grageda, 3-Using molten salts and other liquid sensible storage media in thermal energy storage (TES) systems, in: Advances in Thermal Energy Storage Systems, 2015, pp. 49–63, https://doi.org/10.1533/9781782420965.1.49.
[5] R. Ferri, A. Cammi, D. Mazzei, Molten salt mixture properties in RELAP5 code for thermodynamic solar applications, Int. J. Therm. Sci. 47 (12) (2008) 1676–1687, https://doi.org/10.1016/j.ijthermalsci.2008.01.007.
[6] J. López Sanz, F. Cabello Nuñez, F. Zaversky, Benchmarking analysis of a novel thermocline hybrid thermal energy storage system using steelmaking slag pebbles as packed-bed filler material for central receiver applications, Sol. Energy 188 (2019) 644–654, https://doi.org/10.1016/j.solener.2019.06.028.
[7] D. Brosseau, J.W. Kelton, D. Ray, M. Edgar, K. Chisman, B. Emms, Testing of thermocline filler materials and molten-salt heat transfer fluids for thermal energy storage systems in parabolic trough power plants, J. Sol. Energy Eng. 127 (2005) 109–116, https://doi.org/10.1115/1.1824107.
[8] Z. Yang, S.V. Garimella, Thermal analysis of solar thermal energy storage in a molten-salt thermocline, Sol. Energy 84 (2019) 974–985, https://doi.org/10.1016/j.solener.2010.03.007.
[9] S.S.M. Tehrani, R.A. Taylor, K. Nithyanandam, A.S. Ghazani, Annual comparative performance and cost analysis of high temperature, sensible thermal energy storage systems integrated with a concentrated solar power plant, Solar Energy, V 153 (1) (2017) 153–172, https://doi.org/10.1016/j.solener.2017.05.044.
[10] S. Flueckiger, Z. Yang, S.V. Garimella, An integrated thermal and mechanical investigation of molten-salt thermocline energy storage, Appl. Energy (2011), 20982105, https://doi.org/10.1016/j.apenergy.2010.12.031.
[11] S. Torras, C.D. Perez-Segarra, I. Rodriguez, J. Rigola, A. Oliva, Parametric study of two-tank TES systems for CSP plants, Energy Procedia 69 (2015) 1049–1058, https://doi.org/10.1016/j.egypro.2015.03.206.
[12] F. Cabello Núñez, J. López Sanz, F. Zaversky, Analysis of steel making slag pebbles as filler material for thermocline tanks in a hybrid thermal energy storage system, Solar Energy 188 (2019) 1221–1231, https://doi.org/10.1016/j.solener.2019.07.036.
[13] V.D. Cao, S. Pilehvar, C. Salas-Bringas, A.M. Szczotok, J.F. Rodriguez, M. Carmona, N. Al-Manasir, A. Kjøniksen, Microencapsulated phase change materials for enhancing the thermal performance of Portland cement concrete and geopolymer concrete for passive building applications, Energy Convers. Manag. 133 (2017) 56–66, https://doi.org/10.1016/j.enconman.2016.11.061.
[14] L.F. Cabeza, L. Navarro, A.L. Pisello, L. Olivieri, C. Bartolomé, J. Sánchez, S. Álvarez, J.A. Tenorio, Behaviour of a concrete wall containing micro-

encapsulated PCM after a decade of its construction, Sol. Energy 200 (2020) 108–113, https://doi.org/10.1016/j.solener.2019.12.003.
[15] Y. Liu, M. Xie, E. Xu, X. Gao, Y. Yang, H. Deng, Development of calcium silicate-coated expanded clay based form-stable phase change materials for enhancing thermal and mechanical properties of a cement-based composite, Solar Energy 174 (2018) 24–34, https://doi.org/10.1016/j.solener.2018.08.085.
[16] E. John, M. Hale, P. Selvam, Concrete as a thermal energy storage medium for thermocline solar energy storage systems, Sol. Energy 96 (2013) 194–204, https://doi.org/10.1016/j.solener.2013.06.033.
[17] M.C. Alonso, J. Vera-Agullo, L. Guerreiro, V. Flor-Laguna, V.M. Sanchez, M. Collares-Pereira, Calcium aluminate-based cement for concrete to be used as thermal energy storage in solar thermal electricity plants, Cem. Concr. Res. 82 (2016) 74–86, https://doi.org/10.1016/j.cemconres.2015.12.013.
[18] V.A. Salomoni, C.E. Majorana, G.M. Giannuzzi, A. Miliozzi, R. Di Maggio, F. Girardi, D. Mele, M. Lucentini, Thermal storage of sensible heat using concrete modules in solar power plants, Sol. Energy 103 (2014) 303–315, https://doi.org/10.1016/j.solener.2014.02.022.
[19] Z. Ma, P. Davenport, R. Zhang, Design analysis of a particle-based thermal energy storage system for concentrating solar power or grid energy storage, J. Energy Storage 29 (2020), 101382.
[20] NewSOL, ORDIS European Commission, New storage latent and sensible concept for highly efficient CSP Plants, in: CORDIS European Commission, 2017. https://cordis.europa.eu/project/id/720985.
[21] S. Relloso, E. Delgado, Experience with molten salt thermal storage in a commercial parabolic trough plant. Andasol-1 commissioning and operation, in: Proceedings of the 15th SolarPACES Conference, Berlin, 2009.
[22] R.I. Dunn, P.J. Hearps, M.N. Wright, Molten-salt power towers: newly commercial concentrating solar storage, Proc. IEEE 100 (2011) 504–515.
[23] A. Bonk, M. Braun, V.A. Sötz, T. Bauer, Solar salt – pushing an old material for energy storage to a new limit, Appl. Energy 262 (2020), 114535, https://doi.org/10.1016/j.apenergy.2020.114535.
[24] A. Maccari, S. Donnola, F. Matino, S. Tamano, Archimede solar energy molten salt parabolic trough demo plant: improvements and second year of operation, AIP Conference Proceedings 1734 (2016), https://doi.org/10.1063/1.4949195. Issue 1.
[25] G. Peiró, C. Prieto, J. Gasia, A. Jové, L. Miró, L.F. Cabeza, Two-tank molten salts thermal energy storage system for solar power plants at pilot plant scale: lessons learnt and recommendations for its design, start-up and operation, Renew. Energy 121 (2018) 236–248. http://hdl.handle.net/10459.1/62358.
[26] J.I. Burgaleta, S. Arias, D. Ramirez, Gemasolar: the first tower thermosolar commercial plant with molten salt storage, 2011.
[27] M. Vaka, R. Walvekar, P. Jagadish, M. Khalid, M.M. Mubarak, H. Panchal, High-temperature molten salt optimisation using mixture design for energy storage application, J. Energy Storage 32 (2020), 101981, https://doi.org/10.1016/j.est.2020.101981.
[28] A.G. Fernández, S. Ushak, H. Galleguillos, F.J. Pérez, Thermal characterisation of an innovative quaternary molten nitrate mixture for energy storage in CSP plants, Solar Energy Mater. Solar Cells 132 (2015) 172–177, https://doi.org/10.1016/j.solmat.2014.08.020.
[29] C.Y. Zhao, Z.G. Wu, Thermal property characterization of a low melting-temperature ternary nitrate salt mixture for thermal energy storage systems, Sol. Energy Mater. Sol. Cells 95 (2011) 3341–3346, https://doi.org/10.1016/j.solmat.2011.07.029.
[30] N. Ren, Y. Wu, C. Ma, L. Sang, Preparation and thermal properties of quaternary mixed nitrate with a low melting point, Solar Energy Mater. Solar Cells 127 (2014) 6–13, https://doi.org/10.1016/j.solmat.2014.03.056.
[31] R.I. Olivares, W. Edwards, LiNO3–NaNO3–KNO3 salt for thermal energy storage: thermal stability evaluation in different atmospheres, Thermochim. Acta 560 (2013) 34–42, https://doi.org/10.1016/j.tca.2013.02.029.
[32] A. Ibrahim, H. Peng, A. Riaz, M. Abdul Basit, U. Rashid, A. Basit, Molten salts in the light of corrosion mitigation strategies and embedded with nanoparticles to enhance the thermophysical properties for CSP plants, Solar Energy Mater. Solar Cells 219 (2021), 110768, https://doi.org/10.1016/j.solmat.2020.110768.
[33] M. Wittmann, M. Schmitz, H.G. Silva, P. Schmidt, G. Doppelbauer, R. Ernst, P. Santamaria, T. Miltkau, D. Golovca, L. Pacheco, HPS2–demonstration of molten salt in parabolic trough plants–design of plant, AIP Conf. Proc. 2126 (2019), 120024, https://doi.org/10.1063/1.5117642.
[34] M. Roig-Flores, T. Lucio-Martin, M.C. Alonso, L. Guerreiro, Evolution of thermo-mechanical properties of concrete with calcium aluminate cement and special aggregates for energy storage, Cem. Concr. Res. 141 (2021), 106323, https://doi.org/10.1016/j.cemconres.2020.106323.
[35] D. Laing, C. Bahl, T. Bauer, M. Fiss, Breidenbach and M.Hempel. N., High-temperature solid-media thermal energy storage for solar thermal power plants, Proc IEEE 100 (2011) 516–524, https://doi.org/10.1109/JPROC.2011.2154290.
[36] Z.P. Bazant, M.F. Kaplan, Concrete at High Temperatures: Material Properties and Mathematical Models, Longman, 1996.
[37] T. Lucio-Martin, M. Roig-Flores, M.C. Alonso, L. Guerreiro, Evolution of thermal conductivity on CAC concrete at high temperatures and during thermal fatigue tests, in: Proceedings of the 6th International Workshop on Concrete Spalling Due to Fire Exposure, 2019.
[38] T. Lucio-Martin, M. Roig-Flores, M. Izquierdo, M.C. Alonso, Thermal conductivity of concrete at high temperatures for thermal energy storage applications: experimental analysis, Sol. Energy 214 (2021) 430–442, https://doi.org/10.1016/j.solener.2020.12.005.
[39] C. Alonso, L. Fernandez, Dehydration and rehydration processes of cement paste exposed to high-temperature environments, J. Mater. Sci. 39 (2004) 3015–3024.
[40] P. Pimienta, R.J. McNamee, J. Mindeguia, Physical Properties and Behaviour of High-performance Concrete at High Temperature, Springer, Edt, 2018.
[41] J. Mindeguia, P. Pimienta, A. Noumowé, M. Kanema, Temperature, pore pressure and mass variation of concrete subjected to high temperature — experimental and numerical discussion on spalling risk, Cem. Concr. Res. 40 (2010) 477–487, https://doi.org/10.1016/j.cemconres.2009.10.011.
[42] M. Zeiml, D. Leithner, P. Lackner, H.A. Mang, How do polypropylene fibres improve the spalling behaviour of in-situ concrete? Cem. Concr. Res. 36 (2006) 929–942.
[43] K. William, K.K. Lee, Y. Xi, G. Xotta, V. Salomoni, Explosive Spalling of Concrete Materials under Extreme Environments, in Anonymous 2nd International Workshop on Concrete Spalling Due to Fire Exposure, in: The Netherlands, Delft, 2011, pp. 227–236.
[44] V. Antonovič, J. Kerienė, R. Boris, M. Aleknevičiu, The effect of temperature on the formation of the hydrated calcium aluminate cement structure, Procedia Eng. 57 (2013) 99–106, https://doi.org/10.1016/j.proeng.2013.04.015.
[45] U. Herrmann, B. Kelly, H. Price, Two-tank molten salt storage for parabolic trough solar power plants, 29, Energy (2004) 883–893, https://doi.org/10.1016/S0360-5442(03)00193-2.
[46] A. Gomes, M. Navas, N. Uranga, T. Paiva, I. Figueira, T.C. Diamantino, High-temperature corrosion performance of austenitic stainless steels type AISI 316L and AISI 321H, in molten solar salt, Sol. Energy v177 (2019) 408–419, https://doi.org/10.1016/j.solener.2018.11.019.
[47] N.D. Lagaros, N. Vasileiou, G. Kazakis, AC# code for solving 3D topology optimization problems using SAP2000, Optim. Eng. 20 (2019) 1–35.
[48] E.L. Wilson, A. Habibullah, SAP 2000 software. Structural analyses and design, version 19, Computer and Structures, Inc. (CSI), Berkeley, 2017.
[49] J. Brnic, G. Turkalj, J. Niu, M. Canadija, D. Lanc, Analysis of experimental data on the behaviour of steel S275JR – reliability of modern design, Mater. Des. 47 (2013) 497–504, https://doi.org/10.1016/j.matdes.2012.12.037.
[50] B. Hahn, D. Valentine, Essential MATLAB for Engineers and Scientists, Academic Press, 2016.
[51] T. Lucio-Martin, SensibleHeat Storage in Cement-based Materials for Solar Thermal Power PlantsInfrastructures, PhD, UC3M, Madrid, July, 2021.
[52] E. Zarza Moya, Innovative working fluids for parabolic trough collectors, in: M. J. Blanco, L.R. Santigosa (Eds.), Advances in Concentrating Solar Thermal Research and Technology, Woodhead Publishing, 2017, pp. 75–106.
[53] A. Bonk, S. Sau, N. Uranga, M. Hernaiz, T. Bauer, Advanced heat transfer fluids for direct molten salt line-focusing CSP plants, Prog. Energy Combust. Sci. 67 (2018) 69–87, https://doi.org/10.1016/j.pecs.2018.02.002.
[54] C. Xu, Z. Wang, Y. He, X. Li, F. Bai, Sensitivity analysis of the numerical study on the thermal performance of a packed-bed molten salt thermocline thermal storage system, Appl. Energy 92 (2012) 65–75, https://doi.org/10.1016/j.apenergy.2011.11.002.
[55] G. Wang, S. Yu, S. Niu, Z. Chen, P. Hu, A comprehensive parametric study on integrated thermal and mechanical performances of molten-salt-based thermocline tank, Appl. Therm. Eng. 170 (2020), 115010, https://doi.org/10.1016/j.applthermaleng.2020.115010.
[56] S. Watanabe, M. Kinoshita, T. Hosokawa, K. Morigaki, K. Nakura, Capacity fade of LiAlyNi1− x− yCoxO2 cathode for lithium-ion batteries during accelerated calendar and cycle life tests (surface analysis of LiAlyNi1− x− yCoxO2 cathode after cycle tests in the restricted depth of discharge ranges), J. Power Sources 258 (2014) 210–217, https://doi.org/10.1016/j.jpowsour.2014.02.018.
[57] S. Watanabe, M. Kinoshita, T. Hosokawa, K. Morigaki, K. Nakura, Capacity fading of LiAlyNi1−x−yCoxO2 cathode for lithium-ion batteries during accelerated calendar and cycle life tests (effect of depth of discharge in charge-discharge cycling on the suppression of the micro-crack generation of LiAlyNi1−x−yCoxO2 particle), J. Power Sources 260 (2014) 50–56, https://doi.org/10.1016/j.jpowsour.2014.02.103.
[58] Y.F. Baba, A. Al Mers, A. Faik, A. Bouatem, New insight into thermocline packed bed energy storage systems: fast algorithm for sizing, J. Energy Storage 44 (Part B) (2021), 103419, https://doi.org/10.1016/j.est.2021.103419.
[59] C. Odenthal, F. Klasing, T. Baue, Parametric study of the thermocline filler concept based on exergy, J. Energy Storage 17 (2018) 56–62, https://doi.org/10.1016/j.est.2018.01.009.
[60] S.M. Flueckiger, S.V. Garimella, Second-law analysis of molten-salt thermal energy storage in thermoclines, Sol. Energy 86 (2012) 1621–1631, https://doi.org/10.1016/j.solener.2012.02.028.